Segmentation of Brain Electrical Activity into Microstates: Model Estimation and Validation

Roberto D. Pascual-Marqui, Christoph M. Michel, and Dietrich Lehmann

Abstract—**A brain microstate is defined as a functional/physiological state of the brain during which specific neural computations are performed. It is characterized uniquely by a fixed spatial distribution of active neuronal generators with time varying intensity. Brain electrical activity is modeled as being composed of a time sequence of nonoverlapping microstates with variable duration. A precise mathematical formulation of the model for evoked potential recordings is presented, where the microstates are represented as normalized vectors constituted by scalp electric potentials due to the underlying generators. An algorithm is developed for estimating the microstates, based on a modified version of the classical k-means clustering method, in which cluster orientations are estimated. Consequently, each instantaneous multichannel evoked potential measurement is classified as belonging to some microstate, thus producing a natural segmentation of brain activity. Use is made of statistical image segmentation techniques for obtaining smooth continuous segments. Time varying intensities are estimated by projecting the measurements onto their corresponding microstates. A goodness of fit statistic for the model is presented. Finally, a method is introduced for estimating the number of microstates, based on nonparametric data-driven statistical resampling techniques.**

I. Introduction

BRAIN electrical activity recordings consist of time varying measurements of the scalp electric potential field, performed for spontaneous activity (EEG) or for evoked or event-related potentials (EP's, ERP's). These recordings reflect the dynamics of the functional state of the brain. The determination of the functional states [27] and their time sequencing constitute an important problem of electrophysiology.

In studies of EP/ERP's, the waveshapes are interpreted as being formed by a sequence of components, each appearing as a peak or trough in the voltage versus time plot, characterized by a certain amplitude and latency value [1]. The different components are assumed to reflect different functional states of the brain, corresponding to different stages of information processing.

Manuscript received November 25, 1993; revised February 1, 1995. This work was supported in part by an International Brain Research Organization (Suisse) Fellowship, by a grant from the Roche Research Foundation (Suisse) (R. D. Pascual-Marqui), and by Swiss National Science Foundation Grant 32-39420.93.

R. D. Pascual-Marqui was with the Cuban Neuroscience Center, Havana, Cuba and the EEG-EP Mapping Laboratory, Department of Neurology, University Hospital, CH-8091 Zurich, Switzerland. He is now with the Functional Brain Mapping Laboratory, Department of Neurology, University Hospital (HCUG), CH-1211 Genève 14, Switzerland.

C. M. Michel was with the EEG-EP Mapping Laboratory, Department of Neurology, University Hospital, CH-8091 Zurich, Switzerland. He is now with the Functional Brain Mapping Laboratory, Department of Neurology, University Hospital (HCUG), CH-1211 Genève 14, Switzerland.

D. Lehmann is with the EEG-EP Mapping Laboratory, Department of Neurology, University Hospital, CH-8091 Zurich, Switzerland.

IEEE Log Number 9411750.

Viewing multichannel records of EP or ERP data as sequences of momentary potential distribution maps instead of waveshapes indicates that certain map configurations persist during extended epochs (time segments) and that they change rapidly to new configurations that are stable again for given time periods [2]. These time segments of stable map configurations presumably reflect the different steps or modes or contents of information processing, i.e., the functional microstates of the brain [3], [4]. Changes in the spatial distribution of the signal correspond to segment changes, and reflect changes of the functional state. On the other hand, the successive occurrence of microstates does not imply that brain information processing is strictly sequential. The underlying mechanism by which the brain enters a microstate with a given neuronal generator distribution may be composed of any number of sequential or parallel physiological subprocesses [28], [29].

In this work it will be assumed, following Lehmann [3], that the distribution of active neuronal generators (without taking into account intensity) characterizes uniquely the functional microstate of the brain. Formally, this feature corresponds to the normalized current density in the brain. The scalp electromagnetic field reflects the source distribution in the brain. Due to the nonuniqueness of the electromagnetic inverse problem, it may occur that different source distributions produce exactly the same scalp field. However, changes in the scalp field are undoubtedly due to changes in the source distribution. Therefore, a microstate is here defined as being characterized by the normalized vector formed by reference free scalp electric potentials (or by magnetic fields). According to the microstate model, brain electrical activity can then be seen as a sequence of nonoverlapping microstates with variable duration and variable intensity dynamics.

Previous literature on the microstate model has treated aspects such as microstate estimation, segmentation, and physiological validation applying sequential methods [2]–[5]. The method that is presented here is not primarily driven by the sequence of the fields; it examines the entire data set at all time points simultaneously. In the present work, some formal mathematical and statistical problems about this model are dealt with and several new results are presented. It extends earlier work for which preliminary results were obtained [6].

This paper is organized as follows. In Section II-A, a precise mathematical-statistical formulation for the microstate model is given. In Section II-B, an algorithm for its estimation is presented, together with a simple goodness of fit statistic. A method for estimating the number of microstates is derived in Section II-C. In Section III, applications of the methods are illustrated with simulated data and with real ERP recordings.

II. The Microstate Model

A. Definition

A geometrical illustration of the microstate model can be constructed based on an EP/ERP recording with N_s electrodes ($N_s > 2$), transformed to the average reference [7]–[9]. Consider the 2-D plane defined by the electric potential measurements on any two electrodes. A single point on this plane corresponds to an instantaneous measurement. Time varying measurements would be represented as a trajectory consisting of a collection of connected points.

On this plane, a brain microstate is characterized by the coordinate vector of a point located at unit distance from the origin. All points lying on the line going from the origin toward the microstate belong to the same microstate, i.e., all these points have a unique normalized scalp electric potential field (the uniqueness is strictly true only in the case of an infinite number of electrodes). Therefore, as long as a trajectory remains on this line, the brain remains in the same microstate. The distance from the origin to a point on this line is directly related to the intensity (or strength) of the neuronal generators corresponding to this microstate, and is also directly related to the global field power (GFP) [8], which is equivalent to the instantaneous standard deviation of the scalp potential measurements. In general, an ideal full trajectory under the microstate hypothesis consists of a finite number of oriented line segments projecting from the coordinate origin.

In mathematical terms, the microstate model for average reference data can be expressed as

$$V_t = \sum_{k=1}^{N_\mu} a_{kt}\Gamma_k \tag{1}$$

where N_μ is the number of different microstates, V_t is an $N_s \times 1$ vector consisting of the scalp electric potential measurements at time instant $t (t = 1 \cdots N_T)$, Γ_k is the normalized $N_s \times 1$ vector representing the k-th microstate, and a_{kt} is the k-th microstate intensity at time instant t.

In order to allow for nonoverlapping microstates at each time instant t, all a_{kt} must be zero except for one. Therefore, at each time instant, the summation in (1) reduces to a single nonzero term, corresponding to a single active microstate. Formally, the following constraints must be satisfied:

$$\left.\begin{array}{ll} a_{k_1 t} \cdot a_{k_2 t} & = 0, \forall k_1 \neq k_2, \forall t \\ \sum_{k=1}^{N_\mu} a_{kt}^2 & \geq 0, \forall t \end{array}\right\}. \tag{2}$$

It should be emphasized that in this model the time evolution of the active microstates are free and unrestricted, in the sense that the full system dynamics can, in general, be nonlinear and nonstationary.

In the statistical model, the simplest case will be considered in which the measurements in (1) are contaminated additively with zero mean random noise, independent and identically distributed for all time instants

$$V_t = \sum_{k=1}^{N_\mu} a_{kt}\Gamma_k + E_t. \tag{3}$$

For average reference data, it will be assumed that the random $N_s \times 1$ vector E_t has a covariance matrix given by $\sigma^2 H$, where $H = I - \mathbf{1}\mathbf{1}'/N_s$ is the linear average reference transformation matrix [6], I is the identity matrix, and $\mathbf{1}$ is a vector of ones.

B. Estimation

For given N_μ, the model parameters can then be estimated by minimizing the functional

$$\mathcal{F} = \frac{1}{N_T(N_s - 1)} \sum_{t=1}^{N_T} \left\| V_t - \sum_{k=1}^{N_\mu} a_{kt}\Gamma_k \right\|^2 \tag{4}$$

with respect to all Γ_k and a_{kt}, under constraints (2). In (4), $\|X\| = \sqrt{X'X}$ denotes the norm of X.

The procedure presented here for estimating the microstates is basically a subspace pattern recognition method [26]. Specifically, it is a modified version of the classical k-means cluster method [10] used in many unsupervised learning pattern recognition applications. It will be termed the N-microstates algorithm in the context of brain electrical activity. Essentially, the algorithm is a grouped variable coordinate descent method [11] consisting of iterations alternating between two basic steps.

In one step, the normalized and linearly independent set of vectors $\Gamma_k (k = 1 \cdots N_\mu)$ is given. The minimum of functional (4) with respect to a_{kt} under constraints (2) is then obtained as follows. The orthogonal squared distance between each measurement vector and each microstate is computed

$$d_{kt}^2 = V_t' \cdot V_t - (V_t' \cdot \Gamma_k)^2. \tag{5}$$

Each measurement is labeled as belonging to that microstate to which it is closest. If L_t denotes the microstate label, then

$$\hat{L}_t = \arg\min_k \{d_{kt}^2\}. \tag{6}$$

The estimator for the nonzero $a_{\kappa t}$, where $\kappa = \hat{L}_t$, is given by

$$\hat{a}_{\kappa t} = V_t' \cdot \Gamma_\kappa. \tag{7}$$

This part of the algorithm, consisting of (5)–(7), is carried out for all vectors V_t.

In the other step, the labels L_t are given, and the minimum of functional (4) with respect to Γ_k under constraints (2) is obtained directly as the normalized eigenvector corresponding to the largest eigenvalue of the matrix

$$S_k = \sum_{t \backslash L_t = k} V_t \cdot V_t'. \tag{8}$$

Note that the summation includes only time points for which $L_t = k$. Therefore,

$$\hat{\Gamma}_k = \arg\max_X X' S_k X, \text{ under constraint } \|X\| = 1. \tag{9}$$

This part of the algorithm is carried out for all microstates.

The algorithm, summarized in Table I, alternates iteratively between groups of (5)–(7) and (8) and (9). The process is started with an initial guess for either the microstates Γ_k or the labels L_t, and is terminated when successive iterates of the functional $\mathcal{F}$ differ negligibly. Note that the minimum of

TABLE I
THE BASIC N-MICROSTATE ALGORITHM

1) Given N_μ, set $\sigma_0^2 = 0$, and set the convergence criterion parameter ε (e.g. $\varepsilon = 10^{-6}$)

2) Select initialization 2a or 2b:

2a) Given Γ_k, k=1.. N_μ, satisfying $\|\Gamma_k\| = 1$ and $(\Gamma_{k1}' \cdot \Gamma_{k2})^2 < 1$ for $k_1 \neq k_2$, go to step 3

2b) Given L_t, t=1.. N_T, taking integer values in the range 1.. N_μ, go to step 4

3) For t=1.. N_T, compute $L_t = \arg\max_k \{(V_t' \cdot \Gamma_k)^2\}$

4) For k=1.. N_μ,

4a) Compute $S_k = \sum_{t:L_t=k} V_t \cdot V_t'$

4b) Compute $\Gamma_k = \arg\max_X X'S_kX$, under constraint $\|X\| = 1$ (note that Γ_k is the normalized eigenvector of S_k with largest eigenvalue)

5) Compute $\sigma_\mu^2 = \sum_{t=1}^{N_T} \{V_t' \cdot V_t - (\Gamma_\kappa' \cdot V_t)^2\} / (N_T(N_s - 1))$, where $\kappa = L_t$

6) If $|\sigma_0^2 - \sigma_\mu^2| \leq \varepsilon\sigma_\mu^2$ then go to 7, otherwise, set $\sigma_0^2 = \sigma_\mu^2$ and go to step 3

7) For t=1.. N_T,

7a) Set $\kappa = L_t$

7b) For k=1.. N_μ, and $k \neq \kappa$, set $a_{kt} = 0$

7c) Compute $a_{\kappa t} = V_t' \cdot \Gamma_\kappa$

8) Compute $R^2 = 1 - \sigma_\mu^2/\sigma_D^2$, where $\sigma_D^2 = \sum_{t=1}^{N_T} V_t' \cdot V_t / (N_T(N_s - 1))$

functional (4) is an estimator for the noise variance σ^2 in (3), and is given by

$$\mathcal{F}_{\min} = \hat{\sigma}_\mu^2 = \sum_{t=1}^{N_T} \left(V_t' \cdot V_t - (\hat{\Gamma}_\kappa' \cdot V_t)^2\right) / (N_T(N_s - 1)) \quad (10)$$

where $\kappa = \hat{L}_t$. A simple goodness of fit measure for the model is then given by the squared correlation coefficient, i.e., the explained variance

$$R^2 = 1 - \hat{\sigma}_\mu^2 / \hat{\sigma}_D^2 \quad (11)$$

where

$$\hat{\sigma}_D^2 = \sum_{t=1}^{N_T} V_t' \cdot V_t / (N_T(N_s - 1)) \quad (12)$$

is the data variance.

The algorithm in Table I does not necessarily guarantee that the absolute minimum of $\mathcal{F}$ (4) will be found. Actually, it is very sensitive to the starting point (initialization), as with many clustering algorithms [12], and may terminate at a local minimum or even at a saddle point. Therefore, in practice, it is restarted several times with different initial microstates, using randomly selected normalized V_t vectors from the data. The results corresponding to the minimum $\mathcal{F}$ among all repetitions is retained. The repetition strategy is not costly since the algorithm is quite efficient computationally, e.g., an implementation running on a 486-based PC, 50-MHz clock rate, for $N_s = 21, N_T = 256$, and $N_\mu = 9$, takes 2 s/iteration, and usually less than 10 iterations for convergence.

Another general problem inherent to all clustering methods is the resolving power with respect to "close" clusters. In the case of the algorithm in Table I, "close" means high linear dependency between microstates. However, the concept of "closeness" is a statistical one since highly collinear microstates can be resolved provided that the noise variance in (3) is sufficiently small. Although this issue will not be treated in the present paper, an objective estimation of the number of microstates (i.e., "clusters") that can be statistically resolved is given in the following subsection.

The estimated label time series $\hat{L}_t$ contains all the necessary information for segmentation, i.e., each measurement at each time instant belongs to only one microstate. However, $\hat{L}_t$ is very noisy at times of low GFP since under such conditions the distances from the measured field to all microstates are small and almost any choice of microstate gives a good fit. In other words, the variance of the estimator for L_t increases with low GFP. Expressed in mathematical terms, when $(V_t' \cdot V_t)$ in (5) is small, d_{kt}^2 is small for all microstates.

Microstates should not change randomly from one time instant to the next. Rather, they should be stable for a certain amount of time until they change. In order to ensure a certain degree of time continuity of each segment, a final relabeling step is carried out, in which a measurement is assigned to that microstate which satisfies two requirements: 1) the distance between the measurement and the microstate should be small, and 2) the majority of the neighboring measurements (nearby in time) should belong to the same microstate. Requirement 1) expresses goodness of fit, while 2) expresses the notion that measurements that are close together in time tend to be in the same microstate.

The compromise between goodness of fit and smoothness can be established in terms of well-known smoothing techniques used in statistics [13]. In this case, for given N_μ and Γ_k $(k = 1 \cdots N_\mu)$, smoothing of the label time series is achieved by minimizing the following functional with respect to L_t:

$$g = \sum_{t=1}^{N_T} \{V_t' \cdot V_t - (\Gamma_\kappa' \cdot V_t)^2 - \lambda N_{b\kappa t}\} \quad (13)$$

where $\kappa = \hat{L}_t, \lambda > 0, b \geq 1$ (integer valued), and $N_{b\kappa t}$ denotes the number of labels equal to κ in the time interval $(t - b)$ to $(t + b)$, excluding time t (special care must be taken in defining the time interval near the boundaries $t = 1$ and $t = N_T$).

The parameter λ in functional (13) controls the weight given to the penalty term for nonsmoothness of the label time series. The parameter b controls the size of the "neighborhood" where the labels should tend to be the same. Note that if λ is set to zero, then minimization of (13) with respect to L_t is equivalent to minimization of functional (4) with respect to a_{kt} under constraints (2), for given Γ_k $(k = 1 \cdots N_\mu)$. This situation produces the usual noisy estimate for L_t. As λ increases, the label time series becomes smoother, but the goodness of fit becomes worse.

Table II presents an algorithm that implements the minimization of functional (13). The algorithm, together with the values suggested for the control parameters b and λ, are based on previous results by Besag [14] in image segmentation studies. Once the new smooth labels have been obtained, new estimates for a_{kt}, σ_μ^2, and R^2 should be recomputed, using (7), (10), and (11), respectively. An objective approach for estimating λ and b can be based on cross-validation (see the discussion of Besag's paper by Titterington in [14]). However, the actual implementation is close to impractical due to the extremely high computational demand.

TABLE II
THE SEGMENTATION SMOOTHING ALGORITHM

1) Given N_μ and Γ_k (k=1.. N_μ), set $\sigma_0^2 = 0$, set window size parameter b (e.g. $b = 3$), set non-smoothness penalty parameter λ (e.g. $\lambda = 5$), and set the convergence criterion parameter ε (e.g. $\varepsilon = 10^{-6}$)

2) For t=1.. N_T, compute $L_t = \arg\max_k \left\{ \left(V_t' \cdot \Gamma_k \right)^2 \right\}$

3) For t=1.. N_T, set $\Lambda_t = L_t$

4) Compute $e = \sum_{t=1}^{N_T} \left(V_t' V_t - \left(\Gamma_\kappa' \cdot V_t \right)^2 \right) / \left(N_T (N_s - 1) \right)$, where $\kappa = L_t$

5) For t=(1+b) to (N_T -b),

5a) For k=1 to N_μ, compute $N_{bk} = \sum_{\tau=t-b}^{t+b} \delta(L_\tau, k)$, where $\delta(x,y) = \begin{cases} 1 \text{ if } x = y \\ 0 \text{ otherwise} \end{cases}$

5b)Compute $\Lambda_t = \arg\min_k \left\{ \left(V_t' V_t - \left(\Gamma_k' \cdot V_t \right)^2 \right) / \left(2e(N_s - 1) \right) - \lambda N_{bk} \right\}$

6) For t=1.. N_T, set $L_t = \Lambda_t$

7) Compute $\sigma_\mu^2 = \sum_{t=1}^{N_T} \left(V_t' V_t - \left(\Gamma_\kappa' \cdot V_t \right)^2 \right) / \left(N_T (N_s - 1) \right)$, where $\kappa = L_t$

8) If $\left| \sigma_0^2 - \sigma_\mu^2 \right| \le \varepsilon \sigma_\mu^2$ then go to step 9, otherwise, set $\sigma_0^2 = \sigma_\mu^2$ and go to step 5

9) For t=1.. N_T,

9a) Set $\kappa = L_t$

9b) For k=1.. N_μ, and $k \neq \kappa$, set $a_{kt} = 0$

9c) Compute $a_{\kappa t} = V_t' \cdot \Gamma_\kappa$

10) Compute $R^2 = 1 - \sigma_\mu^2 / \sigma_D^2$, where $\sigma_D^2 = \sum_{t=1}^{N_T} V_t' V_t / \left(N_T (N_s - 1) \right)$

C. Validation

The previous subsection treated the model estimation problem for the case when the number of microstates was known *a priori*. In this subsection, the estimation of N_μ, i.e., the model validation problem, will be handled.

The goodness of fit statistic R^2 (11) by itself gives no information about N_μ. It is a monotonic increasing function of N_μ, meaning that the larger the number of assumed microstates, the better the fit to the data. A classical statistical approach for estimating N_μ, based on the R^2 statistic and its probability density, can be summarized as follows: 1) set $N_\mu = 1$; 2) estimate the microstate model and the corresponding R^2 statistic; 3) test $H_0: R^2 = 0$ versus $H_1: R^2 > 0$; 4) if H_0 is rejected, then stop, otherwise set $N_\mu = N_\mu + 1$ and go to step 2). Theoretically, this process terminates at the correct N_μ value. However, there is a great practical difficulty with this approach since the probability density for R^2 under the microstate model is presently unknown, and furthermore, it seems to be quite complicated to calculate.

An alternative methodology for estimating N_μ is based on the use of resampling techniques [15]. They have the advantage over parametric methods, such as the one previously described, of requiring very few statistical assumptions. Furthermore, they are very appealing in the sense that they are data driven. The main intuitive ideas underlying the cross-validation methodology can be appreciated by analyzing the problem of selecting the optimum number of ordered independent regression variables in a linear model. Another important reason for briefly reviewing this example is that there exists a structural similarity to the microstate model, as will be pointed out later.

Consider the data set D formed by pairs (Y_i, X_{iq}), $i = 1 \cdots N_D$, where Y_i are real valued, X_{iq} are $q \times 1$ vectors, q is the number of ordered independent variables, and q may vary in the range $1 \cdots M$. The familiar linear regression model is $Y_i = X_{iq}' \cdot A_q + \varepsilon_i$, where A_q is the $q \times 1$ vector formed by the regression coefficients, and ε is random noise independent and identically distributed with zero mean and variance σ^2. Stacking the points appropriately for the data set D allows the model to be written as $Y = X_q' \cdot A_q + E$, where Y and E are $N_D \times 1$ vectors, and X_q' is an $N_D \times q$ matrix with rank $(X_q') = q < N_D$. Define the reduced data set D^j formed by pairs (Y_i, X_{iq}), $i = 1, 2, \cdots, j-1, j+1, \ldots, N_D$. Let $\hat{A}_q^j$ denote the least squares estimator for A_q obtained by fitting the model to D^j. For a given number of variables q, the cross-validation residual variance estimator is defined as

$$\hat{\sigma}_{\text{cv}}^2(q) = \sum_{j=1}^{N_D} \| Y_j - X_{jq}' \cdot \hat{A}_q^j \|^2 / N_D. \tag{14}$$

According to the cross-validation criterion, the optimum number of independent regression variables q is chosen as the one that minimizes (14). If the optimum model actually exists, then $\hat{\sigma}_{\text{cv}}^2(q)$ as a function of q has a minimum at the correct value. This is so because $\hat{\sigma}_{\text{cv}}^2(q)$ measures the *predictive* residual variance of the model, and therefore, an incorrect model will only be capable of yielding worse prediction. In contrast, consider the familiar residual variance estimator

$$\hat{\sigma}^2(q) = \sum_{i=1}^{N_D} \| Y_i - X_{iq}' \cdot \hat{A}_q \|^2 / N_D \tag{15}$$

where $\hat{A}_q = (X_q X_q')^{-1} X_q Y$ is the least squares estimator for the full data set D. This nonpredictive statistic is a monotonic decreasing function of q, which by itself gives no information about the optimum number of variables in the regression. Its behavior reflects the fact that the larger the number of variables in the regression, the better the fit.

An improvement over the statistical performance of (14) consists of the rotation-invariant generalized cross-validation residual variance, derived by Golub *et al.* [16]

$$\hat{\sigma}_{\text{gcv}}^2(q) = \hat{\sigma}^2(q) \cdot [N_D^{-1} \cdot \text{tr}(I - X_q'(X_q X_q')^{-1} X_q)]^{-2} \tag{16}$$

where $\hat{\sigma}^2(q)$ is given by (15) and $\text{tr}(M)$ denotes the trace of matrix M. A further advantage of (16) over (14) is its computational simplicity. Since $\text{rank}(X_q') = q$, (16) may be written as

$$\hat{\sigma}_{\text{gcv}}^2(q) = \hat{\sigma}^2(q) \cdot [N_D^{-1} \cdot (N_D - q)]^{-2}. \tag{17}$$

Now consider the general case of reference dependent data V_t^r, $t = 1 \cdots N_T$, which may be viewed as a collection of points in N_s-dimensional space. Upon transforming to average reference data, $V_t = HV_t^r$, the new points will lie in an $(N_s - 1)$ subspace because $\text{rank}(H) = N_s - 1$. However, under the ideal microstate model (1) without additive random noise, and if $N_\mu \le (N_s - 1)$, then the points V_t lie in an N_μ subspace. Therefore, estimating N_μ is equivalent to the estimation of the subspace occupied by the reference independent data. In terms of the eigenvectors of the matrix

$$S = \sum_{t=1}^{N_T} V_t \cdot V_t' / N_T \tag{18}$$

and taking into account the statistical microstate model (3), the data may equivalently be expressed as a linear regression model

$$V_t = \vartheta_q \cdot B_t + E_t \tag{19}$$

where ϑ_q is an $N_s \times q$ matrix whose columns are the first q normalized eigenvectors of S in descending eigenvalue order, B_t are regression coefficients (or factor scores), and E_t is independent of B_t. Note that this model is correct for $q = N_\mu$.

Equation (19) establishes the structural similarity between the linear regression model and the microstate model without constraints (2). For given eigenvectors ϑ_q, the *conditional* generalized cross-validation residual variance for model (19) then is

$$\hat{\sigma}^2_{gcv}(q) = \hat{\sigma}^2_S(q) \cdot [(N_s - 1)^{-1} \cdot (N_s - 1 - q)]^{-2} \tag{20}$$

where

$$\hat{\sigma}^2_S(q) = \sum_{i=q+1}^{N_s - 1} \alpha_i / (N_s - 1) \tag{21}$$

and α_i are the eigenvalues of S (18) in descending order. Note that $\hat{\sigma}^2_S(q)$ is the nonpredictive variance unexplained by the first q eigenvectors. Therefore, one estimator for N_μ is given by the value of q at which the predictive residual variance (20) attains its minimum.

The actual estimation of the microstate model as presented in the previous subsection is performed under two major restrictions: first, microstates do not overlap in time (given by (2)), and second, the label time series producing the segmentation must be smooth (minimization of (13)). Equations (19) and (20) do not include these constraints. Motivated by these arguments, a modified version of the predictive residual variance which explicitly takes into account these features is

$$\hat{\sigma}^2_{mcv}(q) = \hat{\sigma}^2_\mu \cdot [(N_s - 1)^{-1} \cdot (N_s - 1 - q)]^{-2} \tag{22}$$

where $\hat{\sigma}^2_\mu$, given by (10), is the microstate model nonpredictive residual variance for q different microstates. As before, N_μ is estimated as the q value minimizing $\hat{\sigma}^2_{mcv}$.

III. Experimental Results

A. Simulated Data

The performance of the algorithm (Tables I and II) for fitting the microstate model, and the performance of the model validation criteria ((20) and (22)) were evaluated by means of simulated data.

In these experiments, scalp electric potentials were produced according to (1) under restrictions (2) with $N_\mu = 3, N_s = 21, N_T = 256, a_{\kappa t} = \mathbf{U}[-1, 1]$ (independent uniformly distributed pseudorandom numbers between -1 and 1), $\kappa = L_t$, and

$$L_t = \begin{cases} 1 & \text{for } (1 \le t \le 50) \\ 2 & \text{for } (51 \le t \le 100) \\ 3 & \text{for } (101 \le t \le 150) \\ 2 & \text{for } (151 \le t \le 256). \end{cases}$$

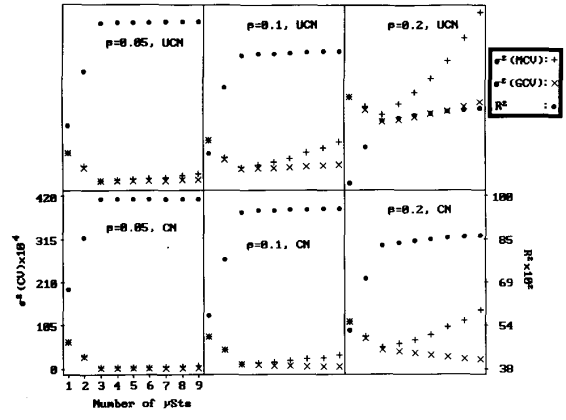

Fig. 1. Modified (σ^2_{mcv}) and generalized (σ^2_{gcv}) cross-validatory criteria and explained variance (R^2), as functions of number of microstates, for synthetic data with $N_\mu = 3$. The six graphs correspond to three different noise variance values ($\beta = 0.05$, 0.1, and 0.2) and two conditions (UCN = uncorrelated noise and CN = correlated noise). μSt = microstates.

The microstate vectors were randomly generated by first setting $\Gamma_{ki} = \mathbf{U}[-1, 1]$, for $k = 1 \cdots N_\mu$ and $i = 1 \cdots N_s$, followed by transformation to common average reference and normalization. The noise vectors in model (3) were obtained as $E_t = \beta H W C_t$, where the $N_s \times 1$ vectors C_t were randomly generated by setting $C_{ti} = \mathbf{U}[-1, 1]$, for $t = 1 \cdots N_T$ and $i = 1 \cdots N_s, W$ is a matrix controlling the noise covariance structure, H is the average reference transformation matrix, and β is a parameter controlling the magnitude of the noise variance.

In a first set of experiments, $W = I$ was used, corresponding to simulated data completely consistent with the statistical microstate model as given by (3), with noise covariance of the form $\sigma^2 H$. This type of covariance structure is likely to result under ideal conditions in which the deviation from model (1) is due to pure instrumental uncorrelated noise.

In a second group of experiments, higher spatial correlation was simulated, obtained by setting

$$W_{ij} = \begin{cases} (1/3) & \text{if } |i - j| \le 1 \\ (1/3) & \text{if } |i - j| = (N_S - 1) \\ 0 & \text{otherwise} \end{cases}$$

for $i, j = 1 \cdots N_s$. Here, the covariance now has the structure $\sigma^2 HWW'H$, which constitutes a violation of the assumptions in model (3). The main motivation for studying the effect of spatially correlated noise is that the most likely source of deviation from the ideal microstate model (1) is biological noise. In other words, if a relatively small fraction of the neuronal generators are not operating according to (1), then the resulting effect is that of spatially correlated deviations, due to the volume conductor effects of the head [17]. It should be emphasized that the main reason for not having treated the more realistic model with additive correlated noise here is the very high complexity of the problem.

Fig. 1 illustrates the main results. The three graphs in the top row correspond to quasi-uncorrelated noise ($\sigma^2 H$). Both cross-validation criteria give the correct estimate for N_μ. However, it should be noted that the modified criterion (22) produces

TABLE III
GENERALIZED (σ^2_{gcv}) AND MODIFIED (σ^2_{mcv}) CROSS-VALIDATORY CRITERIA AND EXPLAINED VARIANCE ($100 \cdot R^2$), AS FUNCTIONS OF NUMBER OF MICROSTATES (N_μ) FOR ERP DATA

N_μ	σ^2_{gcv}	σ^2_{mcv}	$100 \cdot R^2$
1	1.5355	1.5355	53.39
2	0.3481	0.6609	81.99
3	0.2472	0.5137	87.51
4	0.1886	0.4817	89.63
5	0.1537	0.4765	90.98
6	0.1365	0.4973	91.80
7	0.1240	0.5450	92.25
8	0.1167	0.5873	92.88
9	0.1113	0.6681	93.20

a sharper minimum than the generalized version (20). The three graphs in the bottom row were obtained with spatially correlated noise. In this case, the generalized cross-validation criterion breaks down, predicting values for N_μ greater than nine, while the modified criterion produced the correct estimate in all cases. Also included in Fig. 1 is the goodness of fit statistic R^2 as a function of N_μ. As previously discussed, it is seen to be a monotonic increasing function.

With respect to estimation errors, there are two noteworthy results which summarize the situation. First, the lowest correlation coefficient (i.e., the cosine of the angle) between theoretical and estimated microstates was 0.9899. And second, the highest number of errors in the estimated label time series L_t was three (out of $N_T = 256$). In particular, there was, at most, a single misclassified microstate at each segment border. Both results occurred in the high noise level case $\beta = 0.2$, with quasi-uncorrelated noise.

B. ERP Data

Cognitive ERP data with $N_s = 21$ (10/20 international electrode placement system, including electrodes at Oz and at Fpz) were obtained for 12 normal adult subjects (six female and six male). Auditory stimulation was used consisting of 80 dB tones given at 1 m distance from the subjects, with 55 ms duration, and 1044 ms between successive stimuli. Two types of tones (1 and 2 kHz) were presented, randomly ordered, with an asymmetric presentation frequency (20% and 80%), corresponding to two different stimulation conditions. The subjects were required to count the number of rare (less frequent) tones only, in a series of three experiments of 2 min duration each, with 1 min break in between. In half of the subjects (randomly selected), the 1-kHz tone had high presentation frequency. The ERP's were recorded at 250 samples/s, with $N_T = 256$, using amplifiers with high and low pass filters at 0.1 and 40 Hz.

Two average ERP's (averages over stimuli and over subjects), corresponding to the frequent and rare conditions, were analyzed as follows. First, the algorithm in Table I was applied to the two ERP's merged into a single data set with $N_T = 512$. This step produced the microstate estimators common to both ERP's. Second, the algorithm in Table II

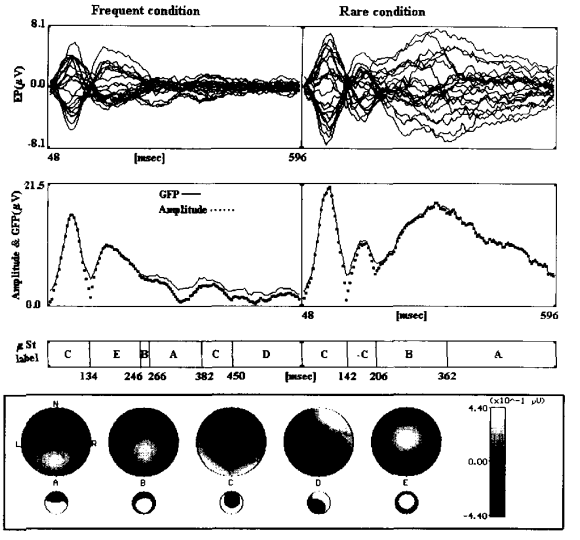

Fig. 2. Segmentation analysis results for ERP data under frequent (left) and rare (right) conditions. Top: superimposed average reference ERP recordings for 21 electrodes (stimulus presentation at $t = 0$). Middle: GFP and estimated microstate amplitude curves (or equivalently, fitted GFP). Bottom: estimated label time series for $N_\mu = 5$ (microstates are labeled **A** to **E**, including polarity). Bottom inset: scalp electric potential maps for normalized average reference microstates, viewed from the top of the head with the indicated orientation (N: nasion; L: left ear; R: right ear), with the smaller map indicating negative polarity in black. μSt = microstates.

was applied separately to each ERP in order to obtain the respective label and strength time series estimators. Finally, the goodness of fit measures were computed over the whole data set, i.e., for $N_T = 512$. This whole process was repeated for N_μ values ranging from 1 to 9. Table III presents the generalized and modified predictive residual variances and the squared correlation coefficient, as a function of the number of microstates. Only the modified criterion (22) produces an estimator for the number of microstates ($N_\mu = 5$) within the explored range ($1 \leq N_\mu \leq 9$).

Fig. 2 illustrates the global field power (GFP) curves and the segmentation results obtained with $N_\mu = 5$. The major features to note here are the following:

1) In both conditions, the early part of the ERP's (up to approximately 140 ms) have the same microstate, but with higher GFP for the rare condition. This first segment, with maximum GFP at approximately 100 ms, corresponds to the auditory $N1$ component [1]. The second segment has a GFP peak at approximately 160 ms, corresponding to the $P2$ component. Different microstates were found in the second segment for the two ERP's, with stronger central positivity for the frequent condition. ERP amplitude differences in the auditory $N1$-$P2$ complex is a classical observation [18], [19]. As can be seen, our method can differentiate amplitude and topography effects. It should be emphasized here that for EP/ERP's in general, polarity is significant from a functional point of view, i.e., even if the microstate had remained the same (as in the first and second segments of the rare ERP in Fig. 2), polarity reversal of the strength (a_{kt}) indicates a change of the functional brain state.

2) The rare condition ERP has the expected large P_{300} component [20], with maximum GFP at approximately 330 ms. However, this classical endogenous component is divided into two segments, the change occurring at approximately 370 ms, and corresponding to two distinct microstates. This result is in agreement with studies of the P_{300} component made by Friedman *et al.* [21], who argued about the existence of "early" and "late" subcomponents with different scalp electric potential distributions and different roles in terms of information processing. Further support to the physiological validity of the results obtained here is found in earlier studies of the P_{300} component, in different experiments performed by Michel *et al.* [4], [22], using other segmentation techniques which also produced two segments for this component.
3) The frequent condition ERP has a very small P_{300}, as expected [20], both in terms of intensity (GFP) and duration.

The foregoing results were obtained with average EP data across subjects (super-averages). Alternatively, segmentation could be performed for all single subject EP's. This seems to be the preferred method if intersubject variability is high, since averaging may smooth out segment borders and topographies. Fortunately, this does not seem to be the case with our data, where relatively high goodness-of-fit measures (explained variance in the range 86–89%) were obtained by using the estimated super-average microstates on each single subject EP.

IV. Conclusion

Methods are developed in this paper for segmentation of brain electrical activity into microstates and for the estimation of the number of microstates. Tests performed on synthetic data and on real ERP measurements provide strong empirical support for the validity of the methods, both from a statistical and physiological point of view. The methods can be extended in a straightforward manner to include both electric potential and magnetic field measurements of brain activity.

The procedure results in a certain finite number of segments for the whole ERP map series data. Some of these segments might have the same label but appear at different time intervals. The same labels mean that they are treated as having the same map configuration. Whether the configurations are statistically identical over subjects can be tested post hoc by computing spatial correlation coefficients of the mean map between segments. Even if the segment configurations are not statistically different, it does not necessarily imply that they reflect the same functional microstate, because they appear at different times after information input and occupy different *order locations* in the concatenation of microstates. The time in which a segment appears is relevant for the functional significance of the segment. Early segments are more likely to be affected by perceptual manipulations while later segments are mainly influenced by manipulations of the cognitive demands [4]. Therefore, an identical labeling of segments that appear at different times does not automatically mean that they have the same functional relevance. For determining the functional property of a certain segment, comparisons between different experimental conditions have to be performed and the sequence, i.e., the syntax of the segments, has to be examined.

The microstate segmentation approach discussed in this paper for EP/ERP data can also be applied to spontaneous multichannel brain electric activity when disregarding the periodic polarity reversals. Earlier work used a sequential approach for segmentation of spontaneous EEG [23]–[25]. In the present nonsequential approach, however, reoccurrence of a segment with the same label at different times requires testing for statistical difference if functional assumptions about repetitive microstates are pursued. Further, the possibility that successive microstates concatenate into higher order units might also be functionally important in spontaneous EEG and needs to be examined. Classification of related microstates into "super classes," as we suggested earlier [25], should not be considered as final recognition of all brain states that reflect the same function, neither in EP/ERP nor in spontaneous EEG.

References

[1] T. W. Picton, S. A. Hillyard, H. I. Krausz, and R. Galambos, "Human auditory evoked potentials. I: Evaluation of components," *Electroenceph. Clin. Neurophysiol.*, vol. 36, pp. 179–190, 1974.
[2] D. Lehmann and W. Skrandies, "Spatial analysis of evoked potentials in man—A review," *Prog. Neurobiol.*, vol. 23, pp. 227–250, 1984.
[3] D. Lehmann, "Principles of spatial analysis," in *Handbook of Electroencephalography and Clinical Neurophysiology, Revised Series*, A. Gevins and A. Remond, Eds., vol. 1. Amsterdam: Elsevier, 1987, pp. 309–354.
[4] C. M. Michel, B. Henggeler, and D. Lehmann, "42-channel potential map series to visual contrast and stereo stimuli: Perceptual and cognitive event-related segments," *Int. J. Psychophysiol.*, vol. 12, pp. 133–145, 1992.
[5] D. Brandeis and D. Lehmann, "Segments of ERP map series reveal landscape changes with visual attention and subjective contours," *Electroenceph. Clin. Neurophysiol.*, vol. 73, pp. 507–519, 1989.
[6] R. D. Pascual-Marqui, R. Biscay, and P. Valdes, "The physical basis of electrophysiological brain imaging: Exploratory techniques for source localization and waveshape analysis of functional components of electrical brain activity," in *Machinery of the Mind—Data, Theory, and Speculations about Higher Brain Function*, E. R. John, Ed. Boston: Birkhauser, 1990, pp. 435–459.
[7] F. F. Offner, "The EEG as potential mapping: The value of the average monopolar reference," *Electroenceph. Clin. Neurophysiol.*, vol. 2, pp. 213–214, 1950.
[8] D. Lehmann and W. Skrandies, "Reference-free identification of components of checkerboard-evoked multichannel potential fields," *Electroenceph. Clin. Neurophysiol.*, vol. 48, pp. 609–621, 1980.
[9] R. D. Pascual-Marqui and D. Lehmann, "Topographic maps, source localization inference, and the reference electrode: Comments on a paper by Desmedt *et al.*," *Electroenceph. Clin. Neurophysiol.*, vol. 88, pp. 532–533, 1993.
[10] H. C. Andrews, *Introduction to Mathematical Techniques in Pattern Recognition*. New York: Wiley, 1972.
[11] J. Bezdek, R. Hathaway, R. Howard, C. Wilson, and M. Windham, "Local convergence analysis of a grouped variable version of coordinate descent," *J. Opt. Theory Applicat.*, vol. 54, pp. 471–477, 1987.
[12] R. J. Hathaway and J. C. Bezdek, "Recent convergence results for the fuzzy c-means clustering algorithms," *J. Classification*, vol. 5, pp. 237–247, 1988.
[13] D. M. Titterington, "Common structure of smoothing techniques in statistics," *Int. Statist. Rev.*, vol. 53, pp. 141–170, 1985.
[14] J. Besag, "On the statistical analysis of dirty pictures (with discussion)," *J. Roy. Statist., Soc. B*, vol. 48, pp. 259–302, 1986.
[15] B. Efron, *The Jackknife, the Bootstrap, and Other Resampling Plans*. Philadelphia: Soc. Industrial and Applied Mathematics, 1982.
[16] G. H. Golub, M. Heath, and G. Wahba, "Generalized cross-validation as a method for choosing a good ridge parameter," *Technometrics*, vol. 21, pp. 215–223, 1979.
[17] P. L. Nunez, *Electric Fields of the Brain*. New York: Oxford, 1981.
[18] S. A. Hillyard, R. F. Hink, V. L. Schwent, and T. W. Picton, "Electrical signs of selective attention in the human brain," *Science*, vol. 182, pp. 177–180, 1973.
[19] R. Näätänen, "Processing negativity: An evoked-potential reflection of selective attention," *Psycholog. Bullet.*, vol. 92, pp. 605–640, 1982.

[20] T. W. Roth, "Auditory evoked responses to unpredictable stimuli," *Psychophysiol.*, vol. 10, pp. 125–137, 1973.
[21] D. Friedman, H. G. Vaughan, Jr., and L. Erlenmeyer-Kimling, "Multiple late positive potentials in two visual discrimination tasks," *Psychophysiol.*, vol. 18, pp. 635–649, 1981.
[22] C. M. Michel and D. Lehmann, "Single doses of Piracetam affect 42-channel event-related potential microstate maps in a cognitive paradigm," *Neuropsychobiol.*, vol. 28, pp. 212–221, 1993.
[23] D. Lehmann, H. Ozaki, and I. Pal, "EEG alpha map series: Brain microstates by space-oriented adaptive segmentation," *Electroenceph. Clin. Neurophysiol.*, vol. 67, pp. 271–288, 1987.
[24] W. K. Strik and D. Lehmann, "Data-determined window size and space-oriented segmentation of spontaneous EEG map series," *Electroenceph. Clin. Neurophysiol.*, vol. 87, pp. 169–174, 1993.
[25] J. Wackermann, D. Lehmann, C. M. Michel, and W. K. Strik, "Adaptive segmentation of spontaneous EEG map series into spatially defined microstates," *Int. J. Psychophysiol.*, vol. 14, pp. 269–283, 1993.
[26] E. Oja, *Subspace Methods of Pattern Recognition*, Research Studies Press. Letchworth, Herts, England. New York: Wiley, 1983.
[27] W. R. Ashby, *Design for a Brain*. New York: Wiley, 1952.
[28] D. Lehmann, "Microstates of the brain in EEG and ERP mapping studies," in *Springer Series in Brain Dynamics 2*, E. Basar and T. H. Bullock, Eds. Berlin: Springer-Verlag, 1989, pp. 72–83.
[29] ——, "Brain electric fields and brain functional states," in *Springer Proceedings in Physics, Evolution of Dynamical Structures in Complex Systems (vol. 69)*, R. Friedrich and A. Wunderlin, Eds. Berlin: Springer-Verlag, 1992, pp. 235–246.

Roberto D. Pascual-Marqui was born January 15, 1952 in Havana, Cuba. He received the B.S. degree in chemistry from Havana University in 1976, and the Ph.D. degree in neurophysics from the Cuban Neuroscience Center in 1988.

From 1981 to 1992, he worked at the Cuban Neuroscience Center, Havana. In 1992, he joined the EEG-EP Mapping Laboratory, Neurology Department, University Hospital, Zurich. Since 1994, he has been the Maître Assistant at the Functional Brain Mapping Laboratory, Neurology Department, University Hospital, Geneva. His research interests include the inverse problem of electrophysiology (i.e., the computation of the current density throughout the full 3-D brain, based on extracranial EEG/MEG measurements), spatio-temporal modeling of brain electrical activity, and biological neural networks.

Christoph M. Michel was born in August 1959 in Reitnau, Switzerland. He received the M.S. degree in 1984 and the Ph.D. degree in 1988 in natural sciences from the Swiss Federal Institute of Technology in Zurich. His area of specialization was neuropsychophysiology. In 1991, he received a National Science Foundation Grant for a postdoctoral fellowship at the Neuromagnetism Laboratory of the Departments of Physics and Psychology and the Center for Neural Science of New York University.

After Ph.D. work, he became a Research Assistant at the Neurology Department of the University Hospital Zurich, Switzerland. He is now Head of the Functional Brain Mapping Laboratory at the Department of Neurology of the University Hospital of Geneva, Switzerland, where the group's interest focuses on the spatio-temporal localization of higher cognitive functions in the healthy and pathological human brain.

Dietrich Lehmann was born December 3, 1929, in Heidelberg, Germany. He completed medical studies at Heidelberg and Paris, and clinical work at Munich and Freiburg, Germany.

From 1962–1970, he performed brain electrophysiology research at UCLA's Brain Research Institute and the Institute of Visual Sciences, University of the Pacific, San Francisco, CA, where he aided in the development of a 48-channel mapping and spatial analysis of evoked ("ERP") and spontaneous ("EEG") brain electric field data, beginning in 1968. In 1971, he moved to Zurich. Presently, he is a Professor of Clinical Neurophysiology in the EEG-EP Mapping Laboratory of the Department of Neurology, University Hospital, Zurich, and Director of The KEY Institute for Brain-Mind Research, University Hospital of Psychiatry, Zurich, Switzerland. His research interests are centered around human brain electric field properties in relation to normal and pathological perception, cognition, and emotion.